Supplementary information

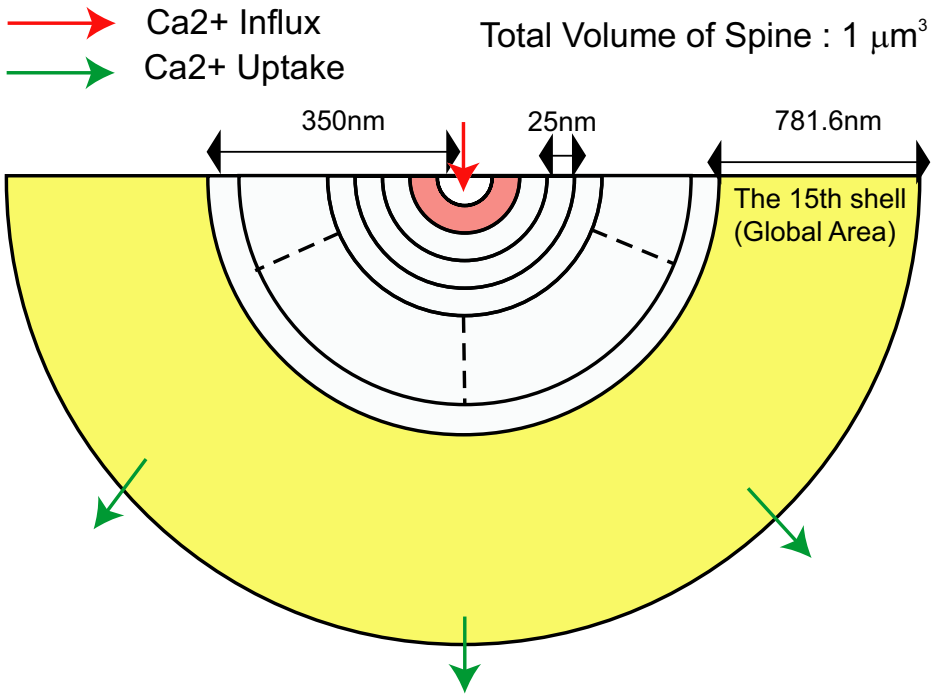

Supplementary Figure 1: A schematic representation of the spatial spine model.

The model spine (1 μm^3) is composed of hemispherical elements (shells) whose thickness is 25 nm (the 1st-14th shells) or 781.6 nm (the 15th shell). When considering the spatial differences in molecular concentration, we compared the 2nd shell (pink, “local”), assumed as the PSD, and the 15th shell (yellow, “global”), assumed as the whole spine. Ca2+ ions are injected through NMDA receptors as a point source located at the center of the 1st shell (red arrow). Ca2+ extrusion by pumps works only in the 15th shell (green arrows).

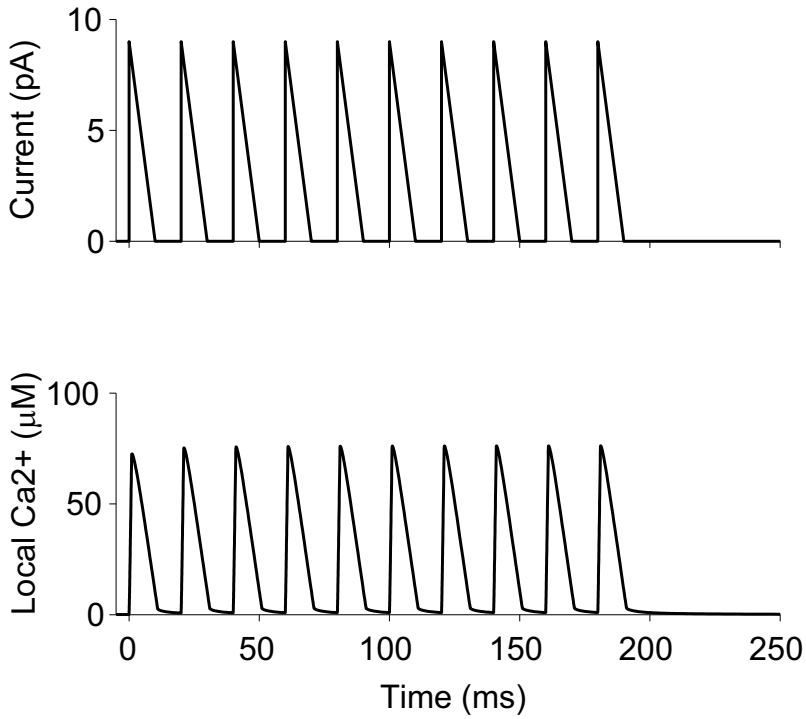

Supplementary Figure 2: Local Ca2+ response when applied triangular-shaped Ca2+ influxes.

(Upper) Temporal pattern of injected currents, whose shape is triangular. The total amount of Ca2+ is half of that by the rectangular-shaped currents shown in Figure 1B.

(Lower) The time course of Ca2+ in the local space (25 – 50 nm away from the NMDARs) in response to the triangular-shaped Ca2+ influxes (Upper). As Figure 2A shows, the shape of local Ca2+ time course reflects the shape of the influx time course.

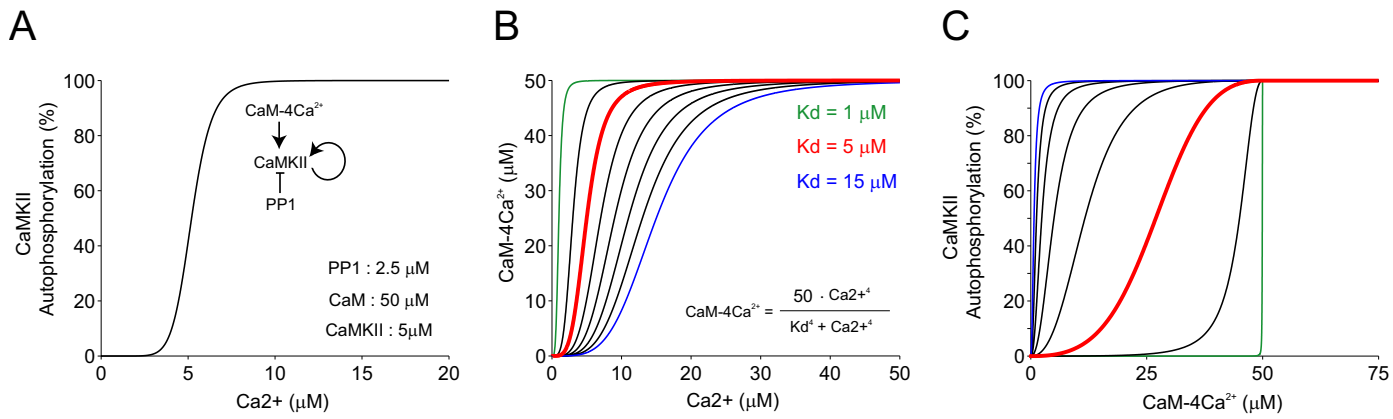

Supplementary Figure 3: Estimation of CaM-4Ca^{2+} levels required for CaMKII activation.

(A) Dose-dependence curve of CaMKII autophosphorylation for Ca2+ in the presence of 50 μM CaM in the condition where the endogenous factor PP1 (2.5 μM) dephosphorylates CaMKII (5 μM). Hill coefficient is 8.9, and half maximum value (Kd) of Ca2+ is 5.2 μM (Bradshaw et al., 2003).

(B) Expected relationship of CaM to Ca2+ for various affinities. In the absence of CaM effectors, the Kd is around 15 μM (Xia and Storm, 2005). In their presence (in the case of (A), the presence of CaMKII), the interaction of one or two Ca2+-bound CaM with CaMKII may increase the CaM affinity with Ca2+, which implies a decrease in Kd (Xia and Storm, 2005). We do not know, however, by how much the Kd value decreases, and thus we plotted several response curves for various CaM affinity values with Ca2+ (by varying Kd from 1 to 15), with the fixed Hill coefficient of 4.

(C) Expected CaM-4Ca^{2+} levels required for CaMKII activation. From (A) and (B), we estimated a probable dose-dependence curve for CaMKII autophosphorylation for CaM-4Ca^{2+}, for various affinity values of CaM with Ca2+. If interaction with CaMKII significantly affects the CaM affinity with Ca2+ (i.e. Kd value becomes small), large CaM activity is required for CaMKII activation. As it turns out, the controllable level of CaM-4Ca^{2+} to activate CaMKII ranges between 0–50 μM, for any CaM affinity with Ca2+. The red line corresponds to the black line in Figure 3A.

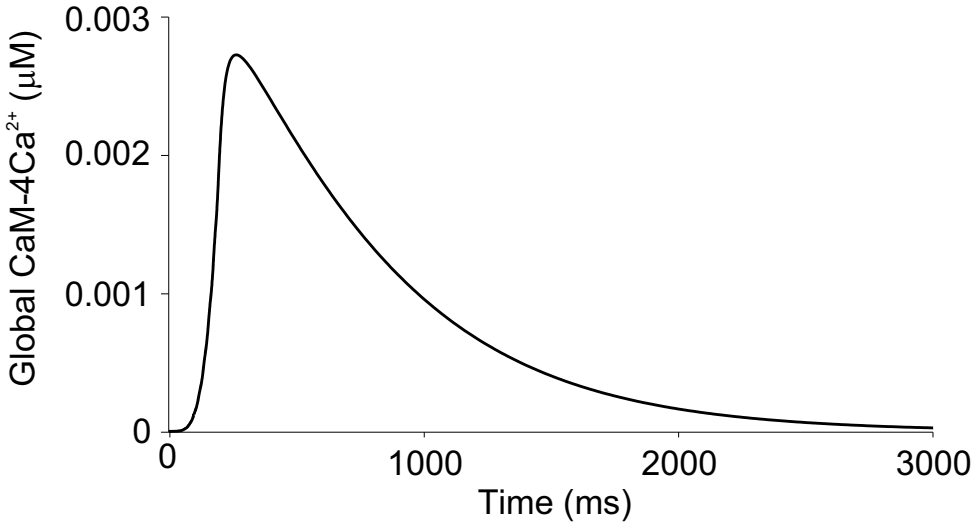

Supplementary Figure 4: Time course of CaM activity in the global area when CaM is non-diffusible. Diffusion coefficient of CaM was set to zero. When the same Ca2+ stimulation as in Figure 1B was applied, the global CaM activation was much less than 0.01 μM, i.e., CaM was not activated.

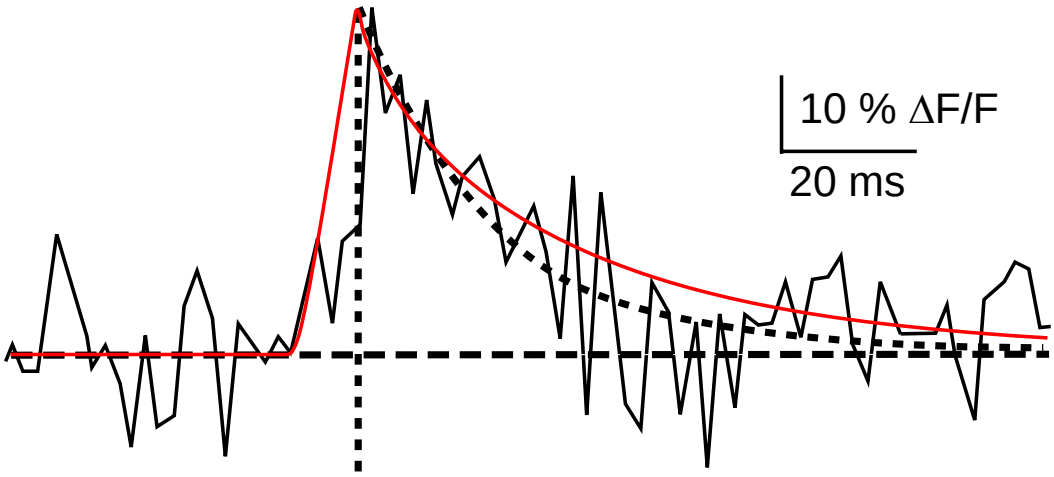

Supplementary Figure 5: Comparison of Ca2+ decay behavior with experimental data.

Solid black line indicates fluorescence change (ΔF/F) corresponding to the Ca2+ response in a dendritic spine, caused by Ca2+ influx through NMDARs, and dotted black line is its smoothed curve (Sabatini et al., 2002). Red line indicates the simulated Ca2+ response when we injected one pulse of Ca2+ stimulation as in Figure 1B. This figure shows that the decay constant of Ca2+ in the simulation is highly consistent with that measured in the Ca2+ imaging study by Sabatini et al. (2002).

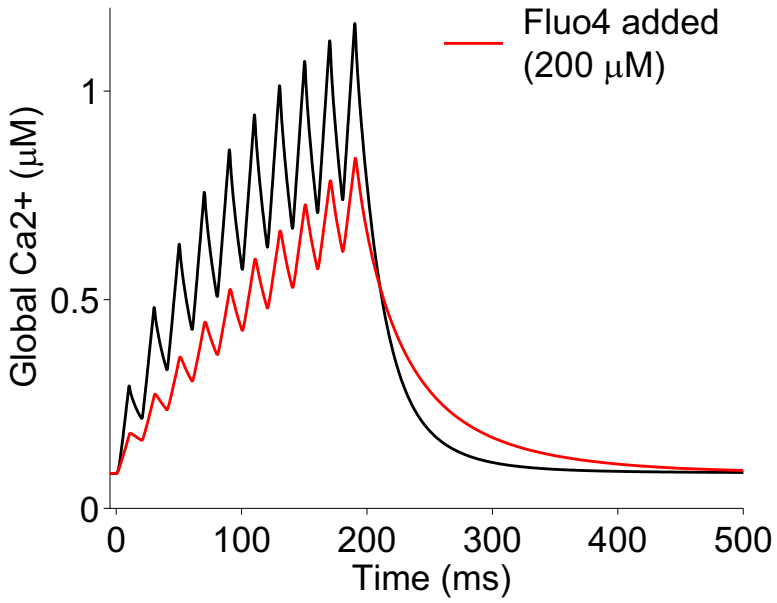

Supplementary Figure 6: Comparison of Ca2+ temporal responses with and without Ca2+ indicator.

Ca2+ stimulation was given as Figure 1B shows. Black and red lines indicate the time courses of global Ca2+ with and without Fluo-4 (200 μM), respectively. With Fluo-4, Ca2+ peak became lower and decay of Ca2+ became slower than in the condition without the indicator. Kf and Kb values of Fluo-4 were set at 1000 $\mu M^{-1}s^{-1}$ and 300 s^{-1}, respectively (Lattanzio and Bartschat, 1991; Maravall et al., 2000). The diffusion coefficient of Fluo-4 was set at 200 $\mu m^2/s$ (Michailova et al., 2002).

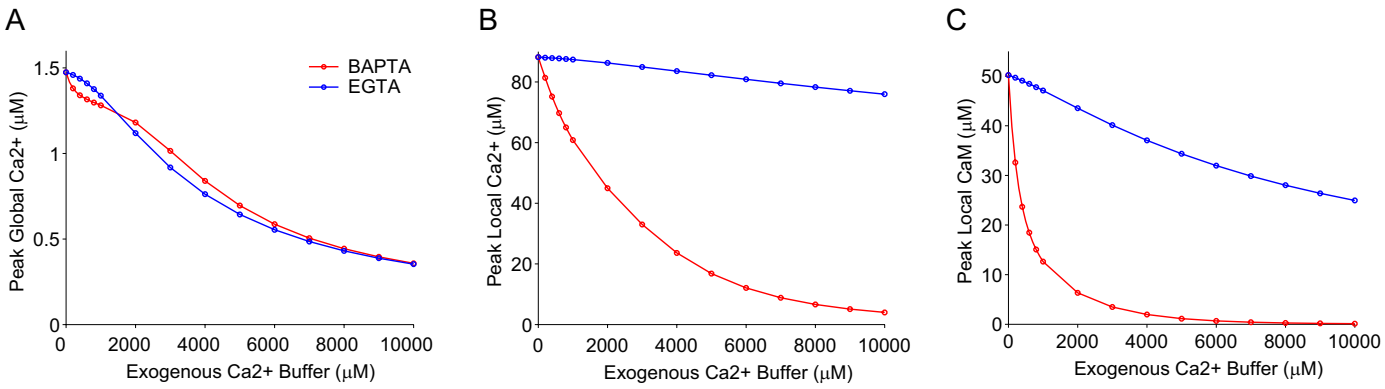

Supplementary Figure 7: Comparison of effects of BAPTA and EGTA on the local and global Ca2+ signaling. Peak responses of global Ca2+ (A), local Ca2+ (B) and local CaM (C) when 100 Ca2+ influxes were applied are plotted against various concentrations of BAPTA (red line) and EGTA (blue line). The frequency and each injected current were the same as shown in Figure 1B. BAPTA and EGTA have been used for checking whether physiological phenomena like synaptic plasticity and pre-synaptic vesicle release are regulated by local Ca2+ signaling or not (Augustine et al., 2003; Hoffman et al., 2002). These two exogenous buffers affect the response in global Ca2+ in a similar manner (A), while BAPTA works significantly in local Ca2+ (B) and local CaM (C). Dissociation rate (Kb/Kf) of these exogenous buffers in Ca2+ binding is almost same, but BAPTA has much faster kinetics than (more than one-hundred times as fast as) EGTA. If a certain phenomenon is regulated by the global Ca2+ signaling, whose dynamics is slow (Figure 2A, lower panel), effects of BAPTA and EGTA are similar, because their dissociation rates are almost same. On the contrary, because the local Ca2+ signaling is rapid and transient (Figure 2A, upper panel), the slow EGTA buffering cannot follow the transient Ca2+ responses, while the fast BAPTA buffering eliminates the Ca2+ nano-domain. Kf, Kb, and diffusion coefficients of these exogenous buffers are 600 $M^{-1}s^{-1}$, 100 s^{-1}, 95 $\mu m^2/s$ for BAPTA (Pethig et al., 1989), and 1.5 $M^{-1}s^{-1}$, 1.3 s^{-1}, 113 $\mu m^2/s$ for EGTA (Tsien, 1980). Actually, an early-phase LTP, which is regulated by local Ca2+ signaling, is attenuated by adding BAPTA or EGTA with different effects with each other, like observed in (B) and (C), while a late-phase LTP, which is globally regulated, is attenuated in a similar manner between by BAPTA and by EGTA, likewise in (A) (Hoffman et al., 2002).

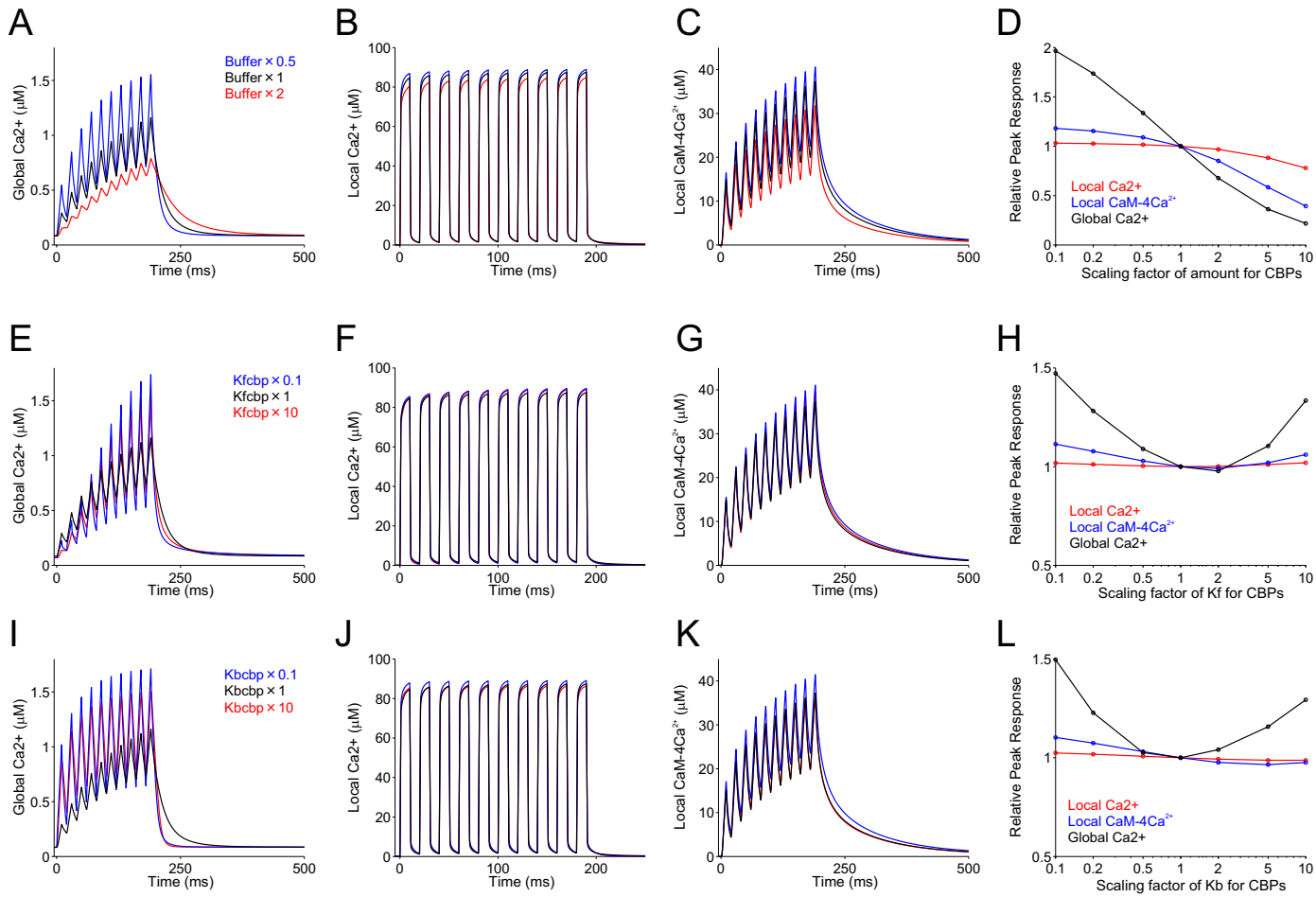

Supplementary Figure 8: Sensitivity of Ca2+ signaling to Ca2+ buffering system.

Local and global signaling was examined when the amount of CBPs and CBP kinetic parameters (Kf, Kb) were changed. Ca2+ stimulation was given as Figure 1B shows.

(A-C) Blue, black, and red lines indicate temporal responses of global Ca2+ (A), local Ca2+ (B), and local CaM activity (C) when the CBP amount was changed as 2, 1, 0.5 times, respectively.

(E-G) Blue, black, and red lines indicate temporal responses of global Ca2+ (E), local Ca2+ (F), and local CaM activity (G), when the Kf value of every CBP was changed as 10, 1, 0.1 times, respectively.

(I-K) Blue, black, and red lines indicate temporal responses of global Ca2+ (A), local Ca2+ (B), and local CaM activity (C), when the Kb value of every CBP was changed as 10, 1, 0.1 times, respectively.

(D, H, L) Black, blue, and red lines indicate the peak responses of global Ca2+, local Ca2+, and local CaM-4Ca2+, respectively, when the CBP amount (D), Kf (H) or Kb (L) value of every CBP was varied as from 0.1 to 10 times.

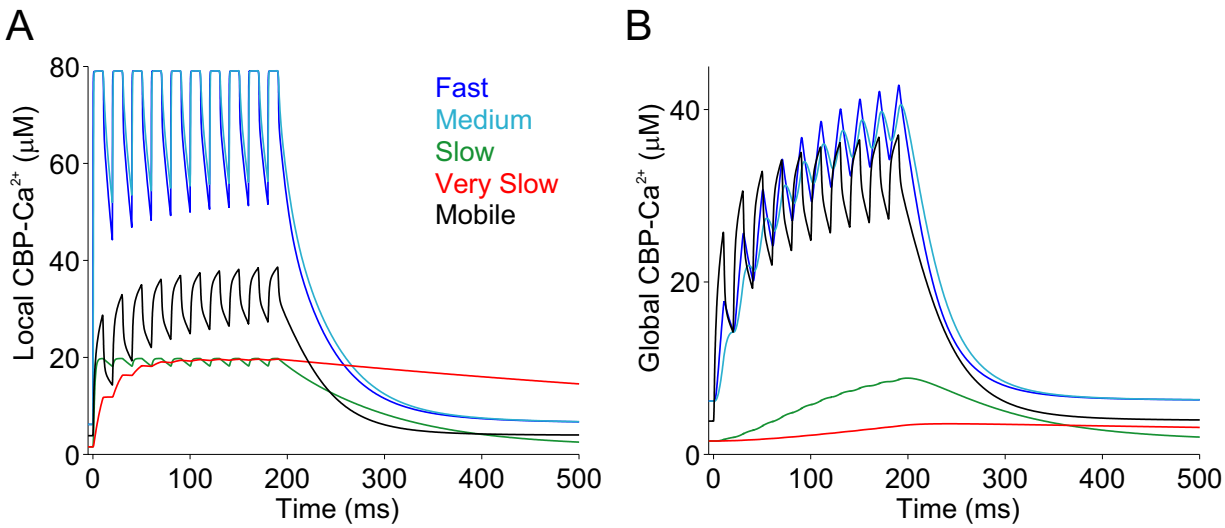

Supplementary Figure 9: Temporal response of CBPs.

The responses of the five kinds of CBPs are shown, when Ca2+ stimulation was given as Figure 1B shows. Blue, cyan, green, red, and black lines indicate Fast, Medium, Slow, Very Slow, and Mobile CBPs, respectively, each bound by Ca2+, in the local (A) and global area (B). In the local area, the binding of Fast and Medium CBPs with Ca2+ was saturated during each injection of the Ca2+ influxes.

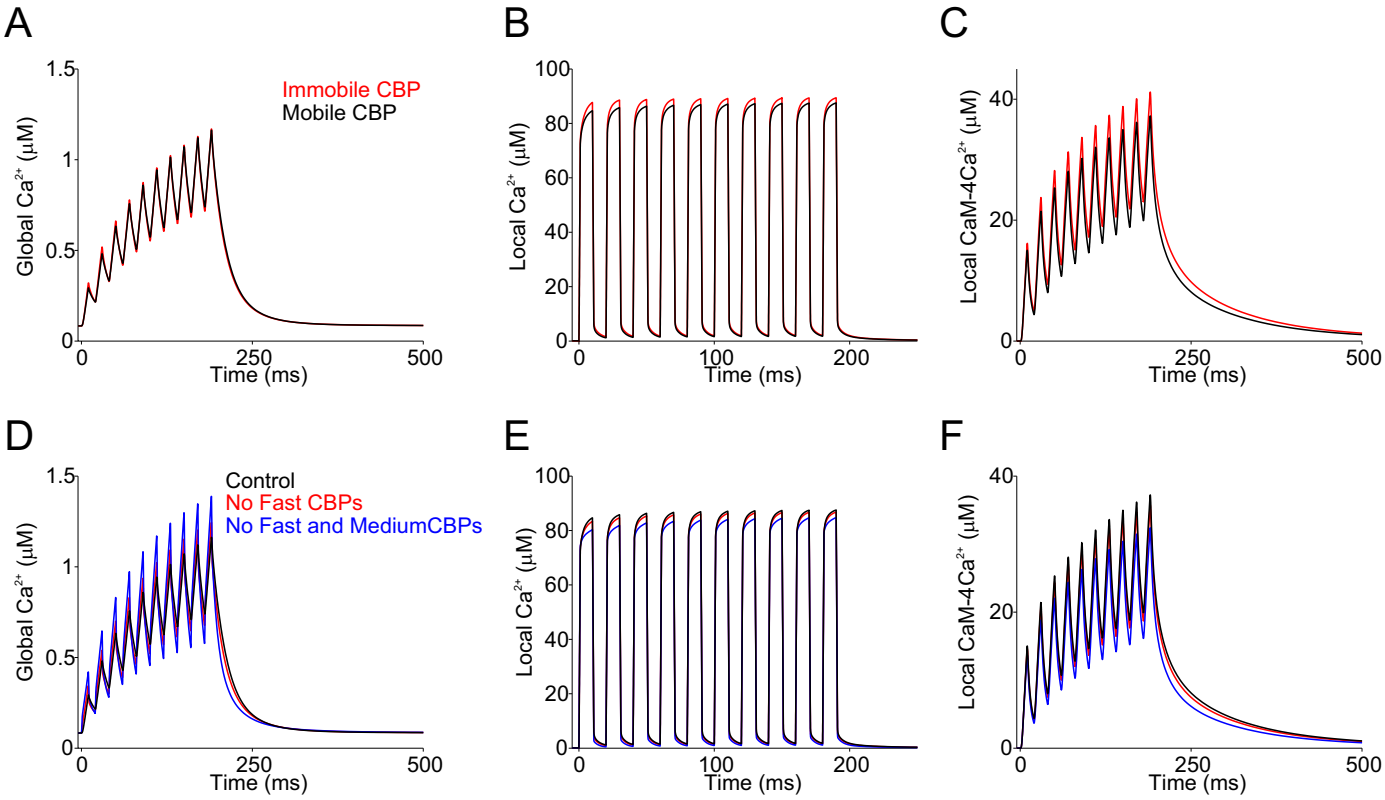

Supplementary Figure 10: Sensitivity of Ca2+ signaling to diffusion of Mobile CBP and to composition of CBPs.

(A-C) To examine if the diffusion of CBP contributes to the Ca2+ dynamics, we compared responses of Ca2+ signaling when "Mobile CBP" was mobile or immobile. Ca2+ stimulation was given as Figure 1B shows. Black and red lines indicate the temporal responses of global Ca2+ (A), local Ca2+ (B), and local CaM activity (C), with and without the diffusion of "Mobile CBP", respectively.

(D-F) To examine the contribution of composition of CBPs to the Ca2+ signaling, especially for Fast and Medium CBPs which showed saturated responses in the local area (Supplementary Figure 9), we changed the composition of CBPs under the condition that the total amount of CBPs was fixed. Ca2+ stimulation was given as Figure 1B shows. Black, red, and blue lines indicate the temporal responses of global Ca2+ (D), local Ca2+ (E), and local CaM activity (F), with Fast and Medium CBPs (control), without Fast CBP, with neither Fast nor Medium CBP, respectively.

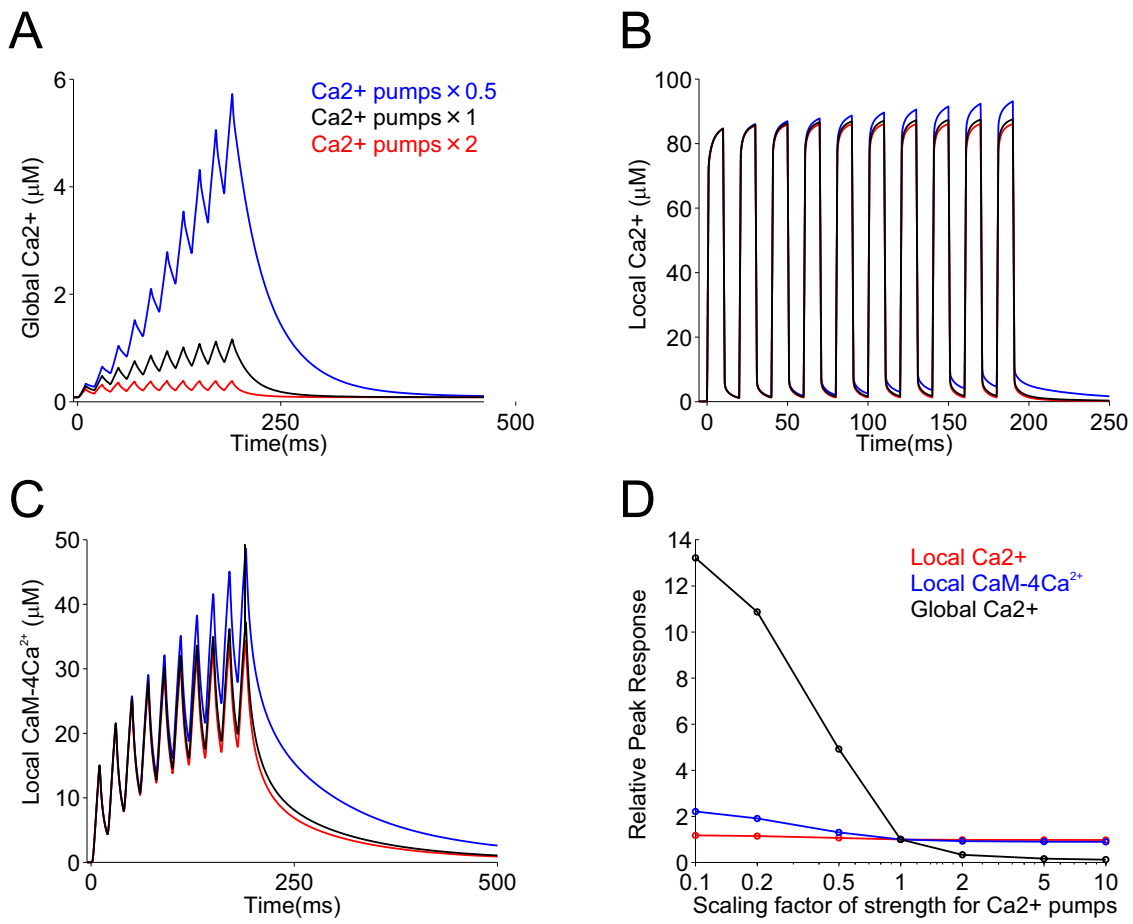

Supplementary Figure 11: Sensitivity of Ca2+ signaling to strength of Ca2+ excretion.

(A-C) Similarly to Supplementary Figure 8 and 10, local and global signaling was examined when the Ca2+ excretion strength was changed. Blue, black, and red lines indicate temporal responses of global Ca2+ (A), local Ca2+ (B), and local CaM activity (C) when the strength of Ca2+ excretion was changed as 2, 1, 0.5 times, respectively.

(D) Black, blue, and red lines indicate the peak responses of global Ca2+, local Ca2+, and local CaM-4Ca2+, respectively, when the strength of all Ca2+ pumps was varied as from 0.1 to 10 times.

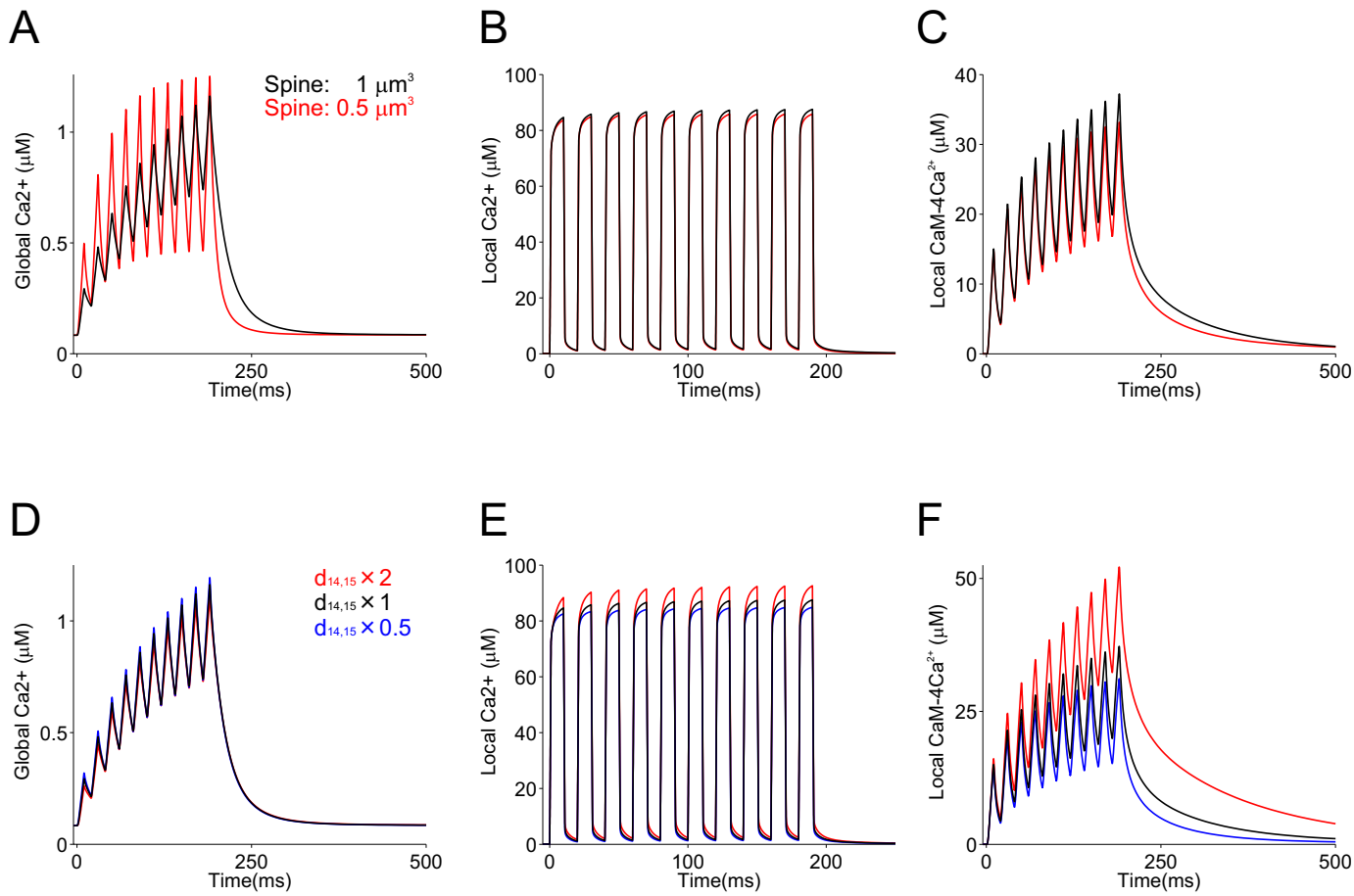

Supplementary Figure 12: Sensitivity of Ca2+ signaling to spine morphology.

(A-C) To examine if the spine size contributes to the Ca2+ dynamics, we compared responses of Ca2+ signaling in the model spine whose volume is 1 μm^3 (black) and 0.5 μm^3 (red). The temporal responses of global Ca2+ (A), local Ca2+ (B), and local CaM activity (C) are shown, when Ca2+ stimulation was given as Figure 1B shows. When the spine volume was 0.5 μm^3, the strength of Ca2+ pumps was increased to 2.5 times so that peak response of global Ca2+ was comparative to that of the 1 μm^3 spine, because it has been known that the peak response of Ca2+ is not correlated with the spine head diameter (Holthoff et al., 2002).

(D-F) To examine if the Ca2+ dynamics are dependent on the spine geometry, we compared responses of Ca2+ signaling when the distance between the 14th and 15th (global area) elements was changed. We assumed the hemi-spherical geometry for the model spine in this study, and this assumption was beneficial not only to making the calculation of diffusion equations easy, but also to enabling us to evaluate the effect from the spine morphology by changing the geometric parameter of the global area (the 15th element). Note that the change in the distance between the 14th and the 15th elements leads to the geometric change of the global area. Ca2+ stimulation was given as Figure 1B shows. Red and blue lines indicate the temporal responses when the distance was changed as 2 and 0.5 times, respectively, and black line that of the control condition, of global Ca2+ (D), local Ca2+ (E), and local CaM activity (F).

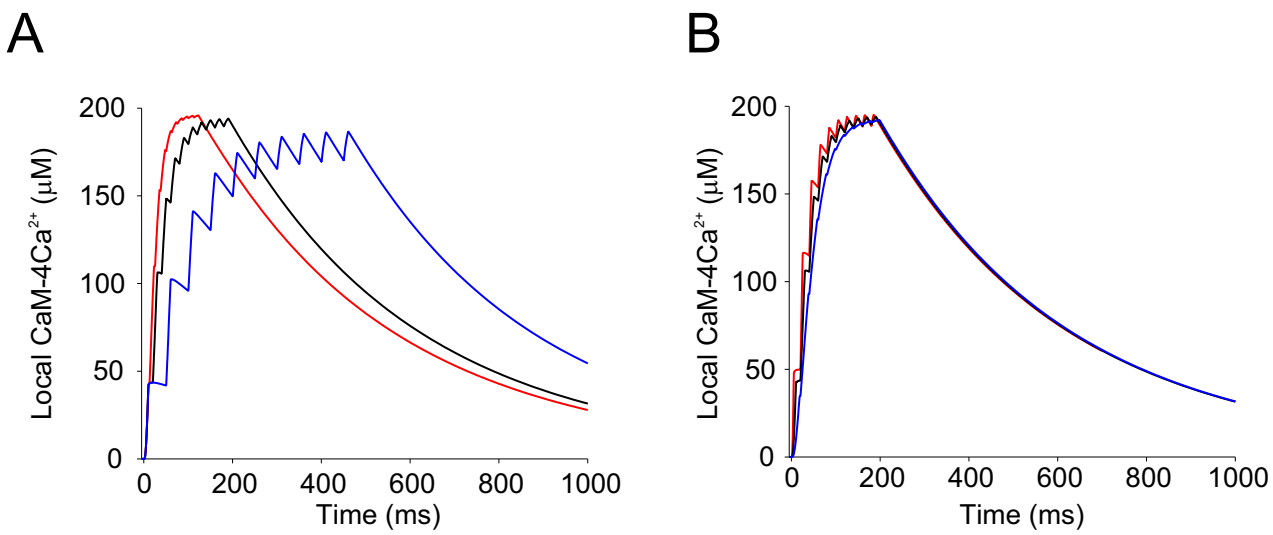

Supplementary Figure 13: The time course of local CaM activity in response to the frequency and the influx rate of Ca2+ influxes when CaM was assumed to be immobile.

(A) The responses of local CaM activity to the three frequency patterns (Figure 4A) when CaM does not diffuse.

(B) The responses of local CaM activity to the three shapes of Ca2+ influx patterns (Figure 4E) when CaM does not diffuse.

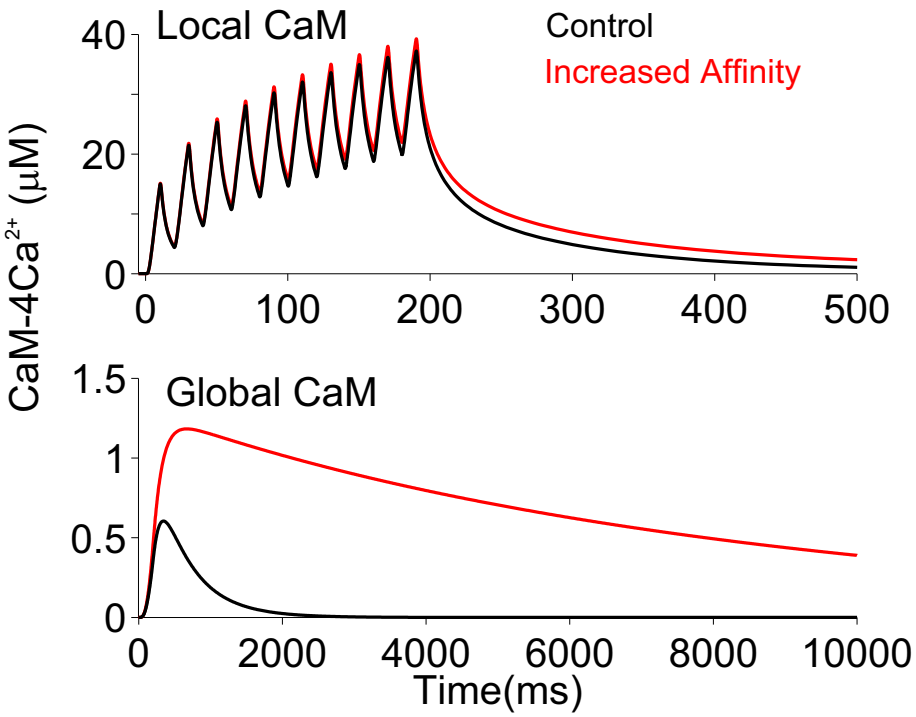

Supplementary Figure 14: Effect of CaM activation on CaM affinity for Ca2+.

Black and red lines indicate local (upper) and global (lower) CaM responses, in the control condition (black line in Figure 5F) and with high CaM affinity for Ca2+ (red line in Figure 5F), respectively.

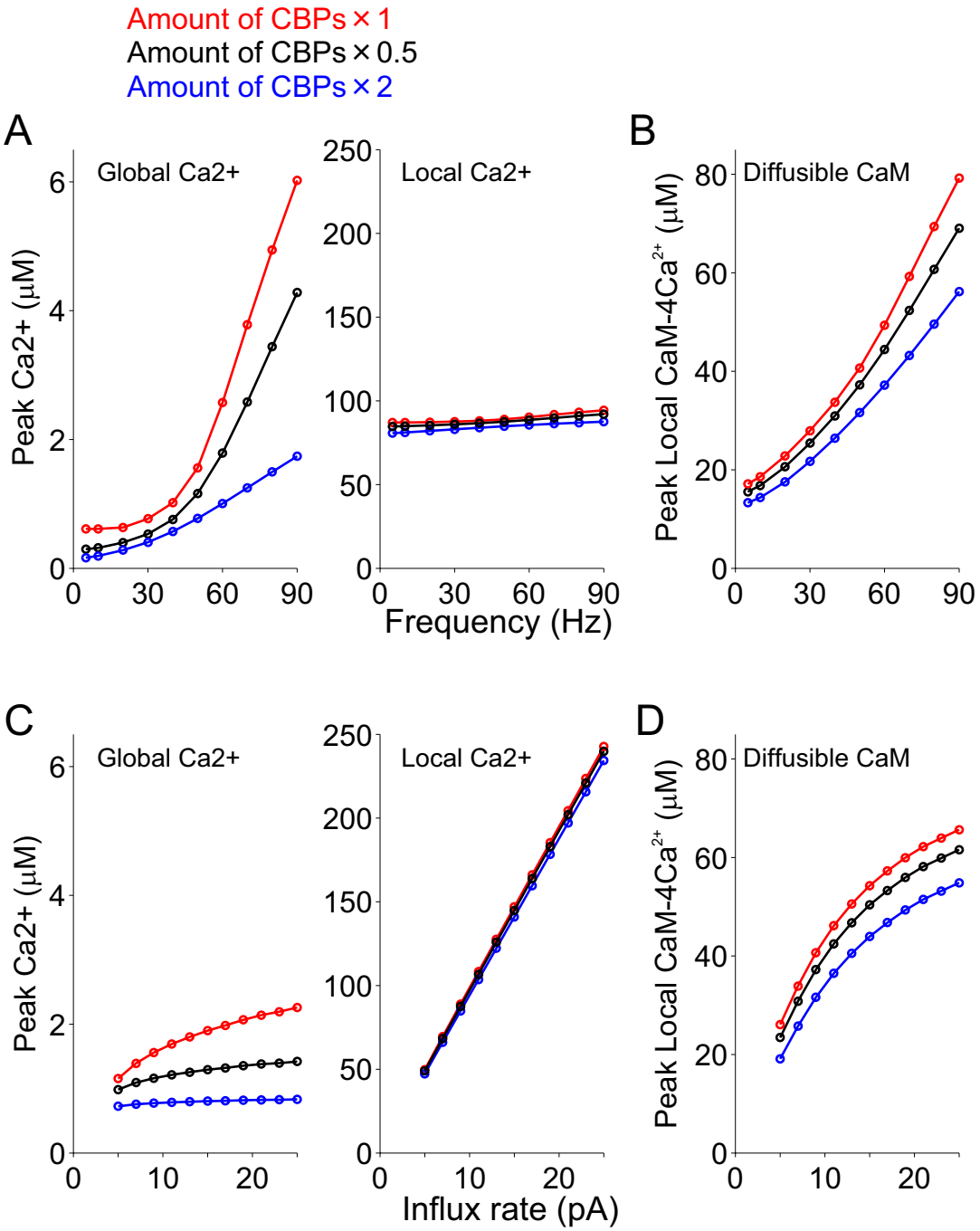

Supplementary Figure 15: Robustness of dual decoding against the amount of CBPs.

Dual decoding property was evaluated, when the amount of CBPs was changed. Blue and red lines indicate the cases that the amount of CBPs was changed as 2 and 0.5 times, respectively, and black line the control condition.

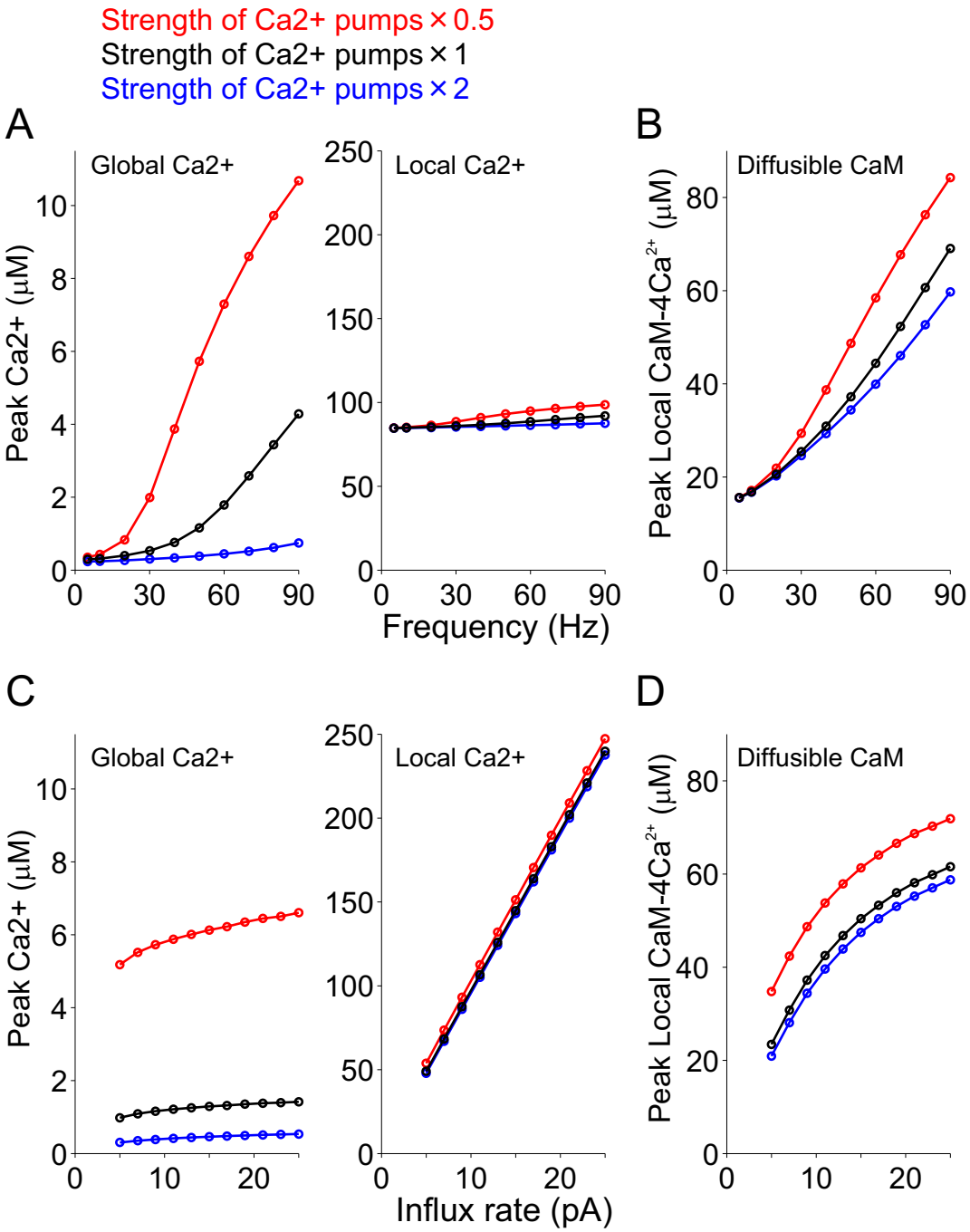

Supplementary Figure 16: Robustness of dual decoding against the strength of Ca2+ pumps.

Dual decoding property was evaluated, when the strength of Ca2+ pumps was changed. Blue and red lines indicate the cases that the strength of Ca2+ pumps was changed as 2 and 0.5 times, respectively, and black line the control condition.

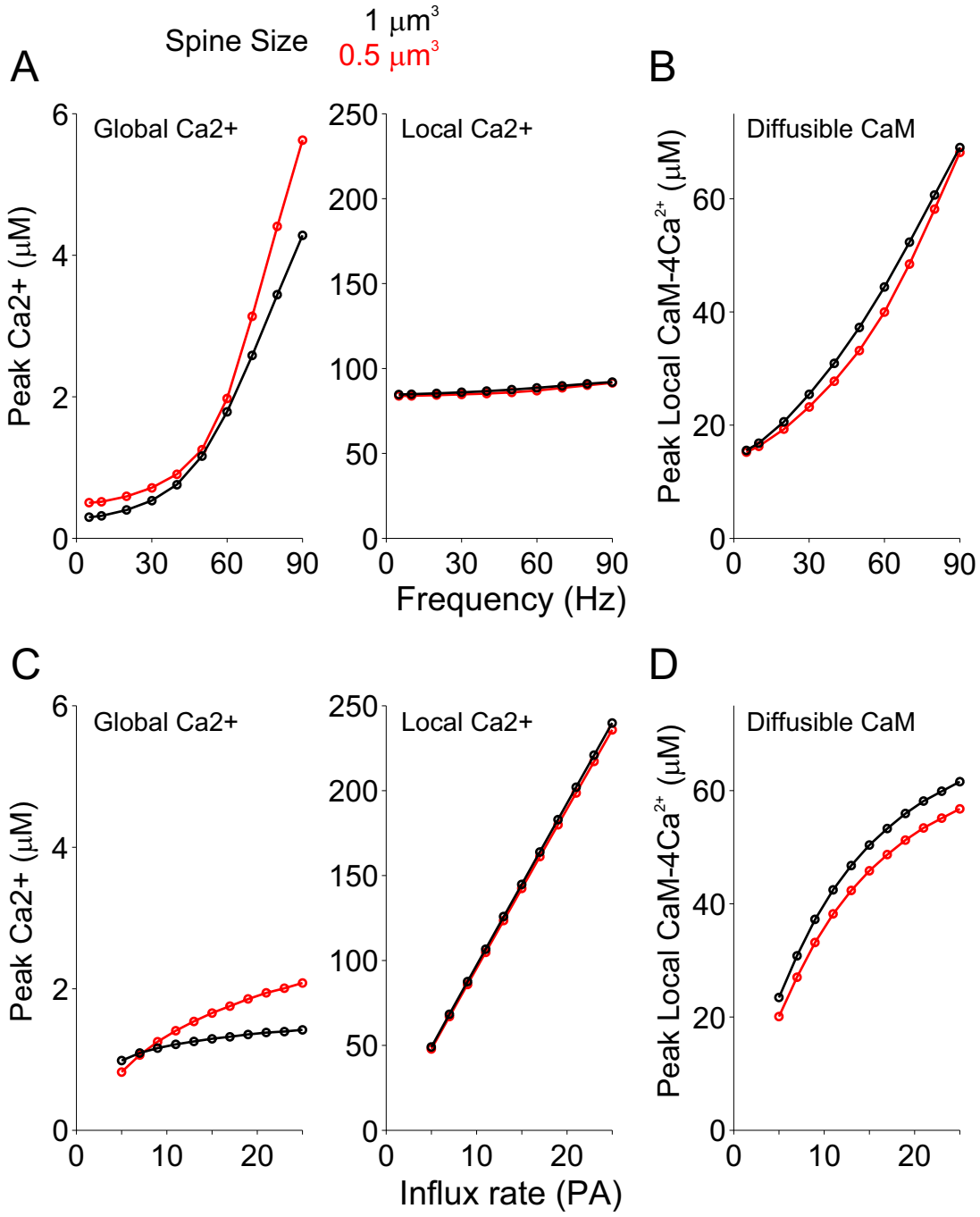

Supplementary Figure 17: Robustness of dual decoding against the spine size.

Dependence of the dual decoding property on the spine size was evaluated. Black and red lines indicate the cases that the spine size was 1 μm^3 and 0.5 μm^3, respectively. For the 0.5 μm^3 spine, the strength of Ca2+ pumps was increased 2.5 times as much as in the control condition (1 μm^3), so that the peak response of global Ca2+ became comparative to the control condition.

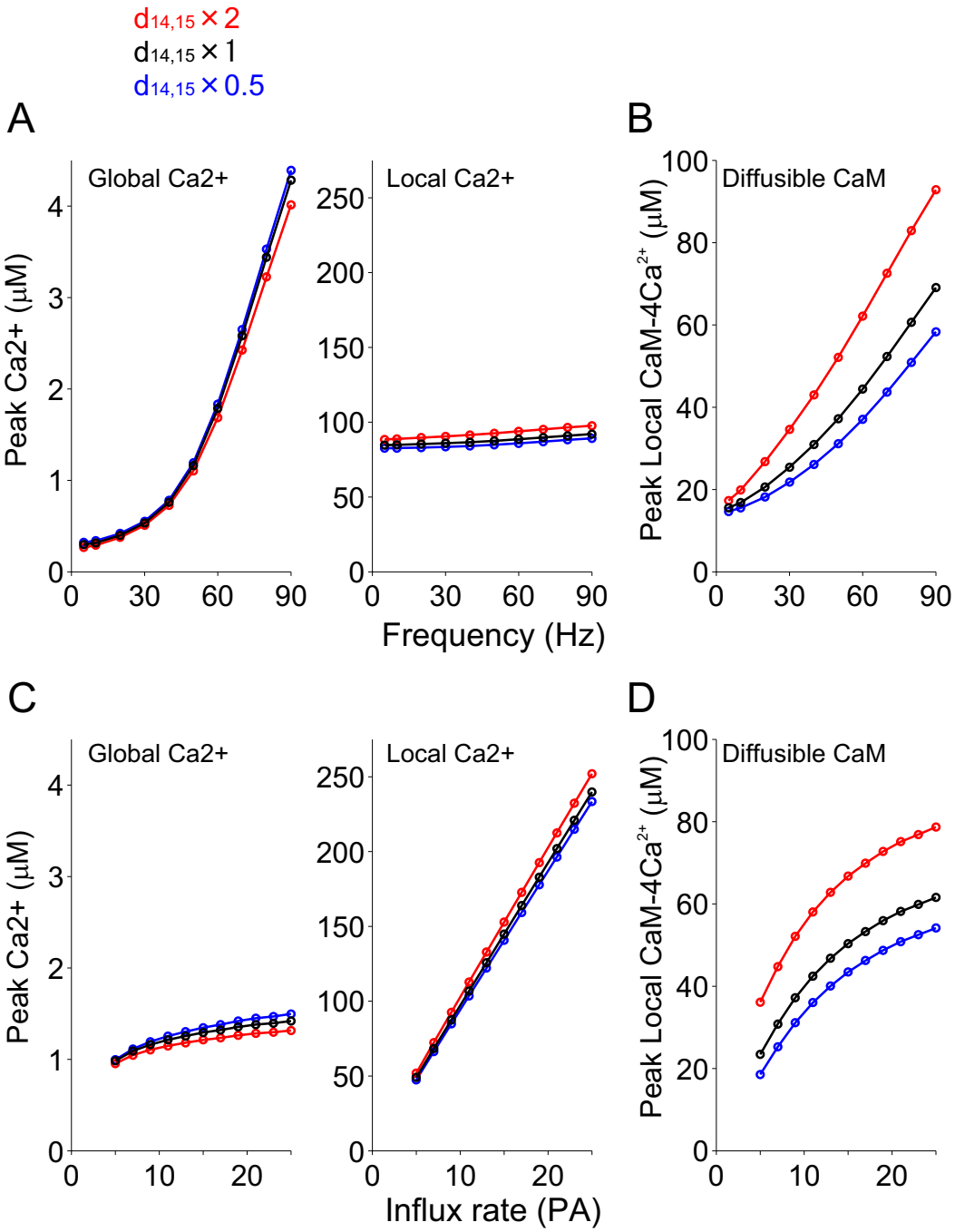

Supplementary Figure 18: Robustness of dual decoding property against the spine geometry.

Dual decoding property was evaluated, when the spine geometry was changed. In the same way as Supplementary Figure 12D-F, we changed the distance between the 14th and 15th (global area) elements. Blue and red lines indicate the cases that the distance was changed as 2 and 0.5 times, respectively, and black line the control condition.

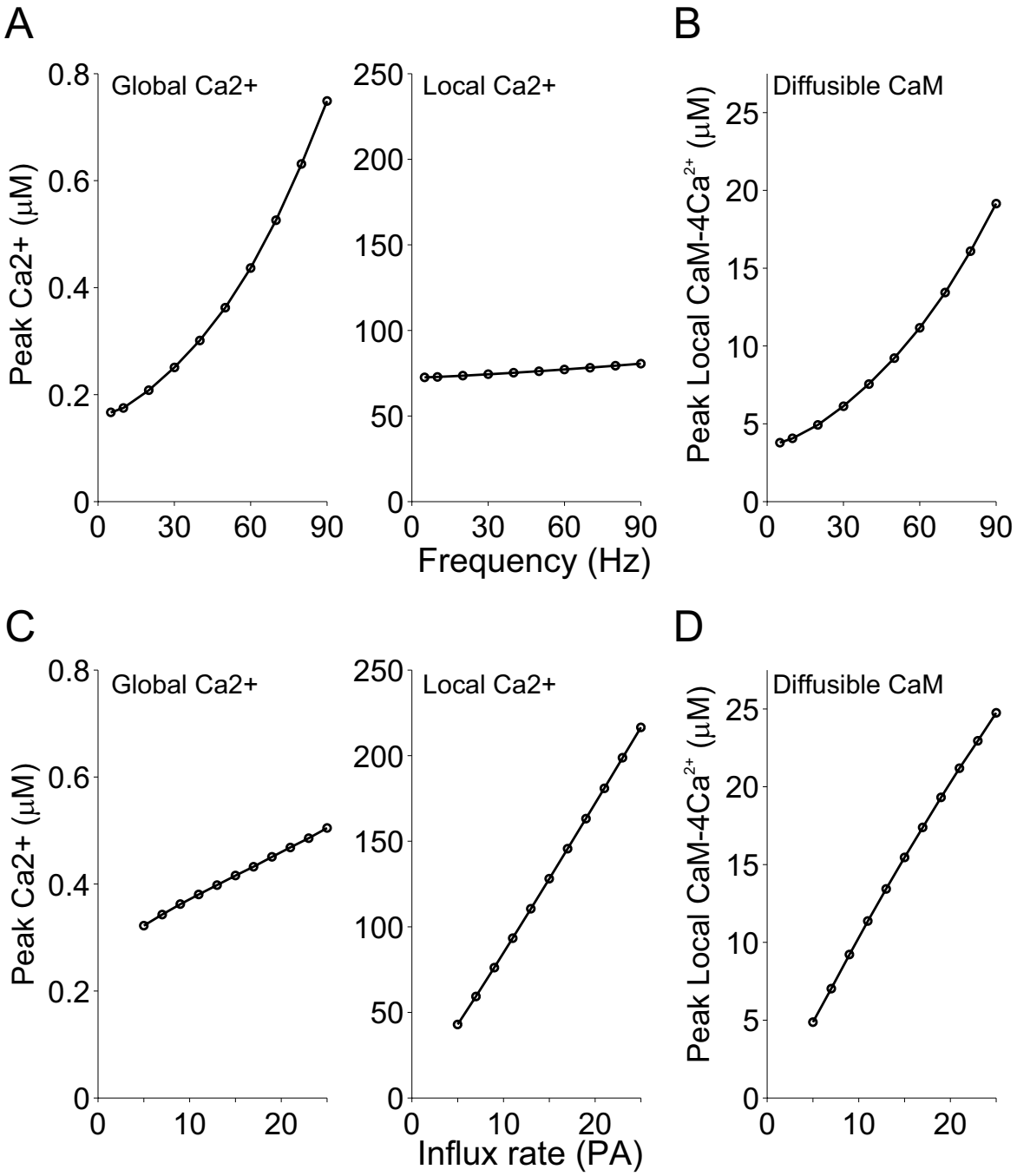

Supplementary Figure 19: Robustness of dual decoding property against the current shapes.

Dual decoding property was evaluated when triangular-shaped Ca2+ influxes (Supplementary Figure 2) were applied, instead of the rectangular ones (Figure 1B, upper panel). Even when triangular-shaped influxes were applied, the dual decoding was maintained, though the responses were relatively low. This result suggests that although Mg2+ block in NMDARs may change the current shapes, whose effect has not been modeled in our study, the dual decoding is accomplished.

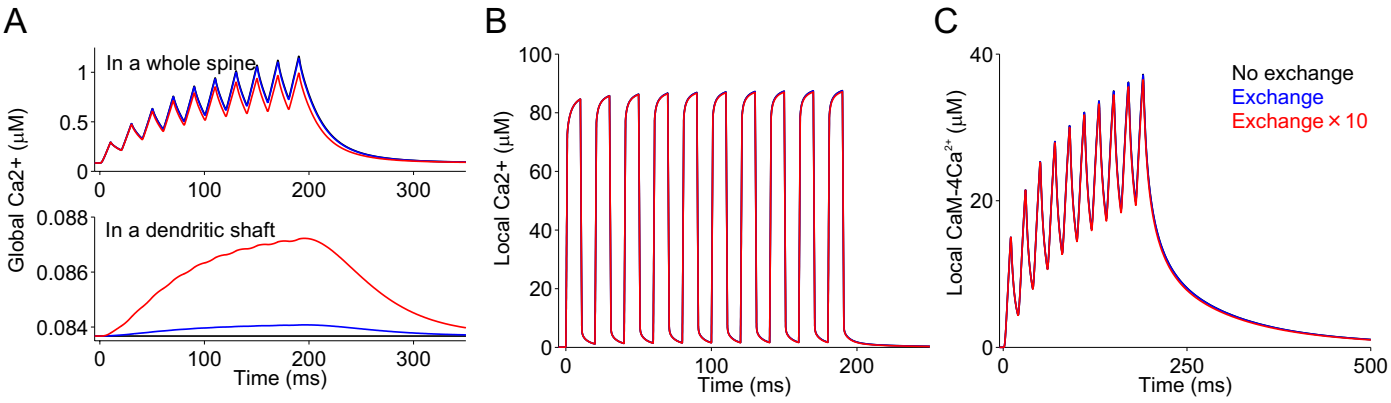

Supplementary Figure 20: Effect of diffusive exchange between a spine and a dendritic shaft on Ca2+ signaling. To determine whether the exchange of Ca2+ and mobile CBPs between a spine and a dendrite affects Ca2+ signaling in a spine, we added one compartment as a dendritic shaft into the model to address the condition of "no exchange". The volume of the additional compartment is assumed to be 5 μm^3. We calculated the exchange through a spine neck whose length and diameter are 0.1 μm and 0.5 μm, respectively. These values are derived from an earlier modeling study (Holmes and Levy, 1990). All Ca2+ regulation in the shaft was the same as those in the spine, so that the resting Ca2+ level became the same as the level in the spine.

(A) Time courses of Ca2+ in the global area of the spine (upper) and the dendritic shaft (lower). Black, blue and red lines indicate, respectively, the Ca2+ time courses without exchange, with exchange, and in the case where the diffusion rate through the spine neck is 10 times greater than the original value.

(B, C) Black, blue and red lines indicate the time courses of local Ca2+ (B) and local CaM activity (C). Line coding is the same as in (A).

Supplementary Table 1. Parameters used in the model			
Parameters		Value	References
<NMDA-R>			
	Current through a single NMDAR	3 pA	(Pina-Crespo and Gibb, 2002)
	Duration of the open state	10 ms	(Pina-Crespo and Gibb, 2002)
	Fraction of current carried by Ca2+	11.00%	(Burnashev et al., 1995)
	Number of NMDARs opened by a single pulse	3	(Nimchinsky et al., 2004)
<Ca2+ ions>			
	Resting Ca2+ concentration	0.08 μM	(Allbritton et al., 1992)
	Diffusion coefficient of free Ca2+	225 $\mu m^2 s^{-1}$	(Kaiser et al., 2001)
<Ca2+ Pumps>			
	Maximal velocity for Na2+/Ca2+ exchanger	3.15 $\mu M s^{-1}$	
	Hill coefficient for Na2+/Ca2+ exchanger	1,7	(Fujioka et al., 2000)
	Half-maximal concentration for Na2+/Ca2+ exchanger	7.3 μM	(Fujioka et al., 2000)
	Maximal velocity for PMCA	1.75 $\mu M s^{-1}$	
	Hill coefficient for PMCA	1	(Stauffer et al., 1995)
	Half-maximal concentration for PMCA	0.2 μM	(Stauffer et al., 1995)
	Maximal velocity for SERCA	2.1 $\mu M s^{-1}$	
	Hill coefficient for SERCA	1.7	(Lytton et al., 1992)
	Half-maximal concentration for SERCA	0.27 μM	(Lytton et al., 1992)
<Ca2+ leakage>			
	Amplitude of Ca2+ leaking from extracellular space	35 s^{-1}	
	Extracellular Ca2+ concentration	2000 μM	
	Amplitude of Ca2+ leaking from the ER	14 s^{-1}	
	Ca2+ concentration in the ER	500 μM	(Park et al., 2000)
<CBP>			
	Total concentration of Fast CBP	80 μM	(Markram et al., 1998)
	Kf for Fast CBP	1000 $\mu M^{-1} s^{-1}$	(Markram et al., 1998)
	Kb for Fast CBP	1000 s^{-1}	(Markram et al., 1998)
	Total concentration of Medium CBP	80 μM	(Markram et al., 1998)
	Kf for Medium CBP	100 $\mu M^{-1} s^{-1}$	(Markram et al., 1998)
	Kb for Medium CBP	100 s^{-1}	(Markram et al., 1998)
	Total concentration of Slow CBP	20 μM	(Markram et al., 1998)
	Kf for Slow CBP	10 $\mu M^{-1} s^{-1}$	(Markram et al., 1998)
	Kb for Slow CBP	10 s^{-1}	(Markram et al., 1998)
	Total concentration of Very-slow CBP	20 μM	(Markram et al., 1998)
	Kf for Very-slow CBP	1 $\mu M^{-1} s^{-1}$	(Markram et al., 1998)
	Kb for Very-slow CBP	1 s^{-1}	(Markram et al., 1998)
	Total concentration of Mobile CBP	50 μM	
	Kf for Mobile CBP	50 $\mu M^{-1} s^{-1}$	
	Kb for Mobile CBP	50 s^{-1}	
	Diffusion coefficient of Mobile CBP	43 $\mu m^2 s^{-1}$	(Schmidt et al., 2003)
<Calmodulin>			
	Total concentration of CaM	200 μM	(Franks et al., 2001)
	Diffusion coefficient of CaM	0.25 $\mu m^2 s^{-1}$	(Luby-Phelps et al., 1995)
	Kf for 1st binding of Ca2+ (N-terminal domain)	16 $\mu M^{-1} s^{-1}$	(Johnson et al., 1996)
	Kb for 1st binding of Ca2+ (N-terminal domain)	405 s^{-1}	(Johnson et al., 1996)
	Kf for 2nd binding of Ca2+ (N-terminal domain)	16 $\mu M^{-1} s^{-1}$	(Johnson et al., 1996)
	Kb for 2nd binding of Ca2+ (N-terminal domain)	405 s^{-1}	(Johnson et al., 1996)
	Kf for 3rd binding of Ca2+ (C-terminal domain)	1.5 $\mu M^{-1} s^{-1}$	(Johnson et al., 1996)
	Kb for 3rd binding of Ca2+ (C-terminal domain)	2.4 s^{-1}	(Johnson et al., 1996)
	Kf for 4th binding of Ca2+ (C-terminal domain)	1.5 $\mu M^{-1} s^{-1}$	(Johnson et al., 1996)
	Kb for 4th binding of Ca2+ (C-terminal domain)	2.4 s^{-1}	(Johnson et al., 1996)

Supplementary References

Allbritton, N.L., Meyer, T. and Stryer, L. (1992) Range of messenger action of calcium ion and inositol 1,4,5-trisphosphate. *Science*, **258**, 1812-1815.

Augustine, G.J., Santamaria, F. and Tanaka, K. (2003) Local calcium signaling in neurons. *Neuron*, **40**, 331-346.

Bradshaw, J.M., Kubota, Y., Meyer, T. and Schulman, H. (2003) An ultrasensitive Ca2+/calmodulin-dependent protein kinase II-protein phosphatase 1 switch facilitates specificity in postsynaptic calcium signaling. *Proc Natl Acad Sci U S A*, **100**, 10512-10517.

Burnashev, N., Zhou, Z., Neher, E. and Sakmann, B. (1995) Fractional calcium currents through recombinant GluR channels of the NMDA, AMPA and kainate receptor subtypes. *J Physiol*, **485 (Pt 2)**, 403-418.

Franks, K.M., Jr, T.M.B. and Sejnowski., T.J. (2001) An MCell model of Calcium dynamics and frequency-dependence of calmodulin activation in dendritic spines. *Neurocomputing*, **38-40**, 9-16.

Fujioka, Y., Hiroe, K. and Matsuoka, S. (2000) Regulation kinetics of Na+-Ca2+ exchange current in guinea-pig ventricular myocytes. *J Physiol*, **529 Pt 3**, 611-623.

Hoffman, D.A., Sprengel, R. and Sakmann, B. (2002) Molecular dissection of hippocampal theta-burst pairing potentiation. *Proc Natl Acad Sci U S A*, **99**, 7740-7745.

Holmes, W.R. and Levy, W.B. (1990) Insights into associative long-term potentiation from computational models of NMDA receptor-mediated calcium influx and intracellular calcium concentration changes. *J Neurophysiol*, **63**, 1148-1168.

Holthoff, K., Tsay, D. and Yuste, R. (2002) Calcium dynamics of spines depend on their dendritic location. *Neuron*, **33**, 425-437.

Johnson, J.D., Snyder, C., Walsh, M. and Flynn, M. (1996) Effects of myosin light chain kinase and peptides on Ca2+ exchange with the N- and C-terminal Ca2+ binding sites of calmodulin. *J Biol Chem*, **271**, 761-767.

Kaiser, K.M., Zilberter, Y. and Sakmann, B. (2001) Back-propagating action potentials mediate calcium signalling in dendrites of bitufted interneurons in layer 2/3 of rat somatosensory cortex. *J Physiol*, **535**, 17-31.

Lattanzio, F.A., Jr. and Bartschat, D.K. (1991) The effect of pH on rate constants, ion selectivity and thermodynamic properties of fluorescent calcium and magnesium indicators. *Biochem Biophys Res Commun*, **177**, 184-191.

Luby-Phelps, K., Hori, M., Phelps, J.M. and Won, D. (1995) Ca(2+)-regulated dynamic compartmentalization of calmodulin in living smooth muscle cells. *J Biol Chem*, **270**, 21532-21538.

Lytton, J., Westlin, M., Burk, S.E., Shull, G.E. and MacLennan, D.H. (1992) Functional comparisons between isoforms of the sarcoplasmic or endoplasmic reticulum family of calcium pumps. *J Biol Chem*, **267**, 14483-14489.

Maravall, M., Mainen, Z.F., Sabatini, B.L. and Svoboda, K. (2000) Estimating intracellular calcium concentrations and buffering without wavelength ratioing. *Biophys J*, **78**, 2655-2667.

Markram, H., Roth, A. and Helmchen, F. (1998) Competitive calcium binding: implications for dendritic calcium signaling. *J Comput Neurosci*, **5**, 331-348.

Michailova, A., DelPrincipe, F., Egger, M. and Niggli, E. (2002) Spatiotemporal features of Ca2+ buffering and diffusion in atrial cardiac myocytes with inhibited sarcoplasmic reticulum. *Biophys J*, **83**, 3134-3151.

Nimchinsky, E.A., Yasuda, R., Oertner, T.G. and Svoboda, K. (2004) The number of glutamate receptors opened by synaptic stimulation in single hippocampal spines. *J Neurosci*, **24**, 2054-2064.

Park, M.K., Petersen, O.H. and Tepikin, A.V. (2000) The endoplasmic reticulum as one continuous Ca(2+) pool: visualization of rapid Ca(2+) movements and equilibration. *Embo J*, **19**, 5729-5739.

Pethig, R., Kuhn, M., Payne, R., Adler, E., Chen, T.H. and Jaffe, L.F. (1989) On the dissociation constants of BAPTA-type calcium buffers. *Cell Calcium*, **10**, 491-498.

Pina-Crespo, J.C. and Gibb, A.J. (2002) Subtypes of NMDA receptors in new-born rat hippocampal granule cells. *J Physiol*, **541**, 41-64.

Sabatini, B.L., Oertner, T.G. and Svoboda, K. (2002) The life cycle of Ca(2+) ions in dendritic spines. *Neuron*, **33**, 439-452.

Schmidt, H., Brown, E.B., Schwaller, B. and Eilers, J. (2003) Diffusional mobility of parvalbumin in spiny dendrites of cerebellar Purkinje neurons quantified by fluorescence recovery after photobleaching. *Biophys J*, **84**, 2599-2608.

Stauffer, T.P., Guerini, D. and Carafoli, E. (1995) Tissue distribution of the four gene products of the plasma membrane Ca2+ pump. A study using specific antibodies. *J Biol Chem*, **270**, 12184-12190.

Tsien, R.Y. (1980) New calcium indicators and buffers with high selectivity against magnesium and protons: design, synthesis, and properties of prototype structures. *Biochemistry*, **19**, 2396-2404.

Xia, Z. and Storm, D.R. (2005) The role of calmodulin as a signal integrator for synaptic plasticity. *Nat Rev Neurosci*, **6**, 267-276.